Spatially-varying Non-stationary Subsurface Motions in Multi-Layered Soil Medium

B. Basu & N.V. Dinh
School of Engineering, Trinity College Dublin, Dublin 2, Ireland

R.B.J. Brinkgreve
Delft University of Technology & Plaxis bv, Delft, The Netherlands

SUMMARY:
This paper presents simulations of spatially-varying non-stationary earthquake motions at subsurface sites in multi-layered soil medium. The motions are compatible to the sites in terms of both spatial-variation and earthquake energy. The stochastic Fourier spectrum characterizes the bedrock energy distribution. The bedrock and subsurface motions are related by a transfer function. The spatial-variation is represented by the existing lagged coherency functional forms and their site-compatible parameters and uniform and random phases. Wavelet transform is introduced to investigate simultaneously the temporal and spectral variation of the simulated motions. In the case study, horizontal motions of three sites at ground surface and at a depth of 20 m in a two layered soil medium above the bedrock depth of 50 m and corresponding to an earthquake moment magnitude of 5.5 are simulated. As subsurface motions are hardly recordable, the simulated motions are useful for the analyses of underground structures and soil-structure interactions.

Keywords: Subsurface motion, spatial-variation, non-stationary, multi-layered soil, wavelet transform.

1. INTRODUCTION

The spatial-variation of ground motions has pronounced effects on structures. Various methods for simulating the spatially-varying ground motions have been developed (Deodatis, 1996; Zerva, 2009; Konakli and Der Kiureghian, 2011 among others). On the subsurface layers, the amplitude and phase of seismic motions at one site are also different from those at other sites. The earthquake-induced motions at subsurface layers are needed for seismic analysis of deep-foundation supported structures and underground structures. However, the records of subsurface motions are hardly obtainable and their simulations are also rarely reported in the literature. Numerical simulations of subsurface motions are therefore necessary and are presented in this paper. The simulation procedure involves characterizing earthquake energy and its loss and amplification, the spatial-variation in amplitude and phase, and the non-stationarity in both time and frequency.

In the literature, the spatial-variation in ground motion amplitude has been represented by various lagged coherency functions with parameters estimated for specific zones. In this paper, the spatial-variation of subsurface motion amplitude is characterized by Harichandran and Vanmarcke (1986) lagged coherency (H-V1986) model with a set of site-compatible parameters. The spatial-variation in phase is characterized by both wave passage effect and arrival time perturbations. The latter caused by the upward travelling variations of the waves and deviations of the propagation pattern has rarely been accounted for. A composite power spectral density (PSD) for earthquake-induced subsurface motions contributed by both the bedrock and the subsurface PSDs is formulated in this paper. The stochastic PSD (Boore, 2003) accounting for the earthquake magnitude, source spectrum and depth, path-dependent loss of energy and geometrical spreading, and source-to-bedrock amplification, is adopted to characterize the earthquake energy at the bedrock. The bedrock and subsurface motions are related by a transfer function derived from vertical propagation of shear waves in multi-layered soil on elastic bedrock. The non-stationarities in both time and frequency of the motions are characterized by the parametric amplitude- and frequency-modulation (Chakraborty and Basu, 2008). The spatially-varying non-stationary ground and subsurface motions are finally simulated by using the one-dimensional

multi-variate (1D-mV) algorithm (Deodatis 1996), which is a non FFT-based algorithm, thus the length of time history is not constrained by the power-of-two.

In order to investigate simultaneously the temporal and spectral variation of the simulated motions, the wavelet transform is used and the Modified Littlewood-Paley (Basu and Gupta, 1998) is chosen as the wavelet basis. In the case study, horizontal motions of three sites at ground surface and at a depth of 20 m in a two layered soil medium above the bedrock depth of 50 m and corresponding to an earthquake moment magnitude of 5.5 are simulated.

2. COMPOSITE PSD OF SUBSURFACE MOTIONS WITH ELASTIC BEDROCK

For simulating spatially-varying non-stationary ground motions, the stationary two-sided PSD function $S(\omega)$ representing the earthquake energy content and has been characterised by Clough-Penzien spectrum (Deodatis, 1996) and by Kanai-Tajimi spectrum (Chakraborty and Basu, 2008) among others. Those spectra were derived using a single-layer soil model. However, real soil medium usually consists of deposits with layers of different stiffness and damping characteristics with boundaries at which elastic wave energy will be reflected and/or be transmitted (Kramer, 1996). In this paper, the geological profile consists of N horizontal layers of soil on an very thick elastic bedrock layer. The PSD of earthquake-induced motions at a subsurface layer n is related to that of bedrock motions by

$$S_n(\omega) = \left|H_n^{\text{soil}}(\omega)\right|^2 S^{\text{bedrock}}(\omega) \tag{1}$$

where, the squared transfer function of the multi-layered soil medium and the PSD of bedrock are expressed respectively as

$$\left|H_n^{\text{soil}}(\omega)\right|^2 = \left|H_{s,n}(\omega)\right|^2 \ldots \left|H_{s,N}(\omega)\right|^2 \tag{2}$$

$$S^{\text{bedrock}}(\omega) = \frac{1}{T_{\text{bedrock}}}\left|F^{\text{bedrock}}(\omega)\right|^2 \tag{3}$$

where T_{bedrock} is the stationary duration of the bedrock stochastic process contributed by the earthquake source and the source-to-bedrock path (Dinh el al., 2012). The transfer function of each soil layer $H_{s,l}(\omega)$, $l = n, \ldots, N$ in Eq. (2) and the Fourier amplitude spectrum of motions at the *top level of the bedrock* (hereby in short called the bedrock) $F^{\text{bedrock}}(\omega)$ in Eq. (3) are formulated in the following sections.

2.1 Transfer Function of Subsurface Layers on Elastic Bedrock

The transfer function relating the acceleration amplitude at the top of layer n to that at the bottom of the layer is given as (Kramer, 1996)

$$H_{s,n}(\omega) = \frac{A_n(\omega) + B_n(\omega)}{A_{n+1}(\omega) + B_{n+1}(\omega)} \tag{4}$$

where A_{n+1} and B_{n+1} are computed from the recursive equations obtained by relating the shear stresses at the top and bottom of layer n

$$A_{n+1}(\omega) = \frac{1}{2}A_n\left(1+\alpha_n^*\right)e^{ik_n^* h_n} + \frac{1}{2}B_n\left(1-\alpha_n^*\right)e^{-ik_n^* h_n} \tag{5}$$

$$B_{n+1}(\omega)=\frac{1}{2}A_n\left(1-\alpha_n^*\right)e^{ik_n^*h_n}+\frac{1}{2}B_n\left(1+\alpha_n^*\right)e^{-ik_n^*h_n} \tag{6}$$

in which, h_n is the thickness of layer n, k_n^* is the complex wave number relating the unit weight ρ_n, shear modulus G_n and damping ratio ξ_n of the soil layer n by

$$k_n^*(\omega)=\omega\sqrt{\frac{\rho_n}{G_n(1+2i\xi_n)}}=\frac{\omega}{V_n\sqrt{1+2i\xi_n}} \tag{7}$$

α_n^* is the complex impedance ratio at the interface between layers n and $n+1$

$$\alpha_n^*(\omega)=\frac{k_n^*G_n(1+2i\xi_n)}{k_{n+1}^*G_{n+1}(1+2i\xi_{n+1})}=\frac{\rho_nV_n}{\rho_{n+1}V_{n+1}}\sqrt{\frac{1+2i\xi_n}{1+2i\xi_{n+1}}} \tag{8}$$

At the ground surface, the shear stress is zero, hence $A_1 = B_1$. It can be assumed without influence on the results that $A_1 = B_1 = 1.0$. Considering the bedrock to be the $(N+1)$th layer and repeating the recursive equations, Eqs. (5) and (6), from the top layer, the complex transfer function of each soil layer, $H_1(\omega)$, …, $H_N(\omega)$, is obtained. The transfer function relating the amplitudes of acceleration at a the top subsurface layer n and bedrock acceleration is

$$H_n^{soil}(\omega)=H_{s,n}(\omega)\ldots H_{s,N}(\omega)=\frac{A_n(\omega)+B_n(\omega)}{A_{N+1}(\omega)+B_{N+1}(\omega)} \tag{9}$$

2.2 Fourier Amplitude Spectrum of Bedrock Motions

The Fourier amplitude spectrum of earthquake motions at bedrock is represented by using the stochastic seismic spectrum (Boore 2003):

$$\left|F^{\text{bedrock}}(\omega)\right|=C\cdot E_s(\omega,M)\cdot G(R)\cdot P(\omega,R)\cdot A(\omega)\cdot D(\omega) \tag{10}$$

where the scaling factor and the source spectrum are respectively expressed as

$$C=\frac{R_eV_eF_s}{4\pi Z_0\rho_0V_{s0}^3} \tag{11}$$

$$E_s(\omega,M)=\omega^2M_0\left\{\frac{1-\varepsilon}{1+\left[\omega/\omega_a(M)\right]^2}+\frac{\varepsilon}{1+\left[\omega/\omega_b(M)\right]^2}\right\} \tag{12}$$

in which, R_e, V_e, F_s, V_{s0} and ρ_0 are respectively the radiation pattern, partition of total shear wave energy into horizontal components, constraint factor, and the shear wave velocity and density of the source rock. The lower corner ω_a frequency relates to the source duration. The term ω_b is the higher corner frequency at which the spectrum attains half of the high frequency amplitude level, and ε is the weighting parameter. The moment magnitude M is mapped from the seismic moment M_0 (dyne-cm). The geometrical spreading function $G(R)$ is characterized by an empirical formulas well supported by data of distance range from 10 to 1000 km with $R=\sqrt{R_0^2+h_e^2}$, R_0 the epi-central distance and h_e the source depth. The term $P(\omega,R)$ is the path-dependent attenuation factor dependent on V_s. The diminution factor $D(\omega)$ accounts for the path-independent attenuation of high-frequency waveforms

and can be represented by the Kappa-filter. The amplification factor $A(\omega)$ is approximated by the source-to-site impedance ratio in a numerical scheme implemented by the authors (Dinh et al., 2012) using the quarter-wavelength approximation method.

3. SIMULATION OF SPATIALLY-VARYING NON-STATIONARY MOTIONS

Earthquake motions at m sites of the subsurface layer n, $u_1(t)$, $u_2(t)$, …, $u_m(t)$, can be considered as components of the one-dimensional multi-variate (1D-mV) non-stationary zero-mean stochastic vector processes having diagonal and off-diagonal elements of the cross-spectra density (CSD) matrix

$$S_{jj}^0(\omega,t) = \left|A_j(\omega,t)\right|^2 S_{n,j}(\omega) \tag{13}$$

$$S_{jk}^0(\omega,t) = A_j(\omega,t)A_k(\omega,t)\sqrt{S_{n,j}(\omega)S_{n,k}(\omega)}\gamma_{jk}(\omega),\ j, k = 1, 2, \ldots, m;\ j \neq k \tag{14}$$

where $A_j(\omega,t)$ is the amplitude- and frequency-modulating function of $u_j(t)$, $\gamma_{jk}(\omega)$ is the complex coherency function between $u_j(t)$ and $u_k(t)$, and $S_{n,j}(\omega)$ is the PSD of earthquake-induced motions at the subsurface layer n presented in Eq. (1).

The 1D-mV algorithm (Deodatis 1996) is introduced to simulate the motions. The CSD matrix is decomposed at every time instant t under consideration as $\mathbf{S}^0(\omega,t) = \mathbf{H}(\omega,t)\mathbf{H}^{T*}(\omega,t)$, where the superscripts T and * denote the matrix transpose and complex conjugate, respectively. Using Cholesky's method, $\mathbf{H}(\omega,t)$ can be evaluated as a lower triangular matrix:

$$\mathbf{H}(\omega,t) = \begin{bmatrix} H_{11}(\omega,t) & 0 & \ldots & 0 \\ H_{21}(\omega,t) & H_{22}(\omega,t) & \ldots & 0 \\ \vdots & \vdots & \ddots & \vdots \\ H_{m1}(\omega,t) & H_{m2}(\omega,t) & \cdots & H_{mm}(\omega,t) \end{bmatrix} \tag{14}$$

The non-stationary vector processes of subsurface motions $u_j(t)$, $j = 1, 2, \ldots, m$, are simulated by using Eqs. (15) where $\omega_l = l\Delta\omega$, $\Delta\omega = \omega_u/N$, ω_u is the upper cut-off frequency beyond which the CSD matrix elements are negligibly small, ϕ_{ml} is the N sequences of independent random phase angles distributed uniformly over $[0, 2\pi]$, and θ_{jm} is the phase angle of the off-diagonal elements of the lower-triangular matrix, $\theta_{jm}(\omega_l,t) = \tan^{-1}\left\{\mathrm{Im}\left[H_{jm}(\omega_l,t)\right]/\mathrm{Re}\left[H_{jm}(\omega_l,t)\right]\right\}$.

$$f_j(t) = 2\sum_{m=1}^{j}\sum_{l=0}^{N-1}\left|H_{jm}(\omega_l,t)\right|\sqrt{\Delta\omega}\cos\Phi(t) \tag{15a}$$

$$\Phi(t) = \omega_l t - \theta_{jm}(\omega_l,t) + \phi_{ml},\ j = 1, 2, \ldots, n \tag{15b}$$

To provide temporal non-stationary, common forms of intensity modulation functions (Zerva, 2009) can be used together with the total duration at a site suggested by the authors (Dinh et al, 2012) that is contributed by both source and path durations. The term $A_j(\omega,t)$ can also be the parametric amplitude- and frequency-modulation function expressed as (Chakraborty and Basu, 2008)

$$A_j(\omega,t) = \lambda_j(\omega)\left[e^{-\beta_j(\omega)t} - e^{-\gamma_j(\omega)t}\right] \tag{16}$$

4. COHERENCY AND SPATIAL-VARIABILITY

The complex coherency function in Eq. (14) is expressed as

$$\gamma_{jk}(\omega) = \left|\gamma(\xi_{jk},\omega)\right| \exp\left[i\,\theta(\xi_{jk},\omega)\right] \tag{17}$$

where the real term $|\gamma(\xi_{jk},\omega)|$, $0 \le |\gamma(\xi_{jk},\omega)| \le 1$ called the lagged coherency characterizes the variation in space and the complex term implies the variation in time. The parameter ξ_{jk} is the separation distance between sites *j* and *k*. The functional form of H-V1986 lagged coherency, Eq. (17), is used with subsurface site parameters estimated by Dinh et al. (2012).

$$\left|\gamma(\xi,f)\right| = A\exp\left[\frac{B(\xi)}{\alpha\sigma(f)}\right] + (1-A)\exp\left[\frac{B(\xi)}{\sigma(f)}\right], \tag{18}$$

$$B(\xi) = -\frac{2\xi}{k}(1-A+\alpha A), \tag{19}$$

$$\sigma(f) = \left[1+\left(\frac{f}{f_0}\right)^{\beta}\right]^{-\frac{1}{2}} \tag{20}$$

Incorporating the wave passage effect of shear waves travelling with velocity V_s and the arrival-time perturbations in the coherency phase gives

$$\theta(\xi_{jk},\omega) = -\omega\left(\frac{\xi_{ik}}{V_s} + \Delta t_{r,jk}\right) \tag{21}$$

where $\Delta t_{r,jk}$ is a normally distributed random variable with zero mean and standard deviation (Boissières and Vanmarcke 1995).

$$\sigma = 2.7\times10^{-2} + 5.41\times10^{-5}\,\xi_{jk}\,[m] \tag{22}$$

5. CONTINUOUS WAVELET TRANSFORM

Continuous wavelet transform can be used to analyze non-stationarity in ground motions (Basu and Gupta, 1998; Chakraborty and Basu, 2008). Consider a "mother" wavelet function, $\psi(t)$, having finite energy. A family of baby wavelets can be constructed by scaling and translating $\psi(t)$ using the dilation (or scale) parameter *'a'* and the translation parameter '*b'* as

$$\psi_{a,b}(t) = \frac{1}{\sqrt{|a|}}\psi\left(\frac{t-b}{a}\right) \tag{23}$$

The parameter *b* localises the basis function at $t = b$ and its neighbourhood, where *a* controls the frequency content of the basis function by stretching or compressing it (with the number of cycles remaining unchanged).

The continuous wavelet transform of the finite energy process $u(t)$ with respect to the basis $\psi(t)$ is obtained by convolving the signal *u(t)* with a set of its baby wavelets

$$W_\psi u(a,b) = \frac{1}{\sqrt{|a|}} \int u(t) \psi^* \left(\frac{t-b}{a} \right) dt \tag{24}$$

where (*) denotes the complex conjugate. Eq. (24) gives the localized frequency information of $u(t)$ around $t = b$. The wavelet transform coefficient, $W_\psi u(a,b)$, represents how well the signal $u(t)$ and the scaled and translated mother wavelet match. More significantly, $W_\psi u(a,b)$ represents the contribution to $u(t)$ in the neighborhood of $t = b$ and in the frequency band corresponding to the value of a. The scale and translation parameters can be numerically assumed as $a_j = \sigma^j$ and $b_i = (i-1)\Delta b$ where σ and Δb are constant parameters.

In this paper, the Modified Littlewood-Paley (MLP) (Basu and Gupta, 1998) is chosen as the wavelet basis because it provides high accuracy in spectral analysis and advantages in numerical computation. The MLP wavelet basis pairs is given by

$$\psi(t) = \frac{1}{\pi \sqrt{2F_1(\sigma - 1)}} \cdot \frac{\sin(2\pi F_1 \sigma t) - \sin(2\pi F_1 t)}{t} \tag{25}$$

$$\begin{aligned} |\hat{\psi}(\omega)| &= \frac{1}{\sqrt{4\pi F_1(\sigma-1)}}, \quad F_1 \le \left|\frac{\omega}{2\pi}\right| \le \sigma F_1 \\ &= \quad 0 \qquad \text{otherwise} \end{aligned} \tag{26}$$

where F_1 is the initial cut-off frequency of the mother wavelet. It is noted by Basu and Gupta (1998) that $\sigma = 2^{1/n}$, $n \ge 4$ is found reasonable based on investigations on several ground motions recorded. However, as small value of σ leads to increased computational effort, $\sigma = 2^{1/4}$ has been chosen.

6. CASE STUDY

In this case study, a geological profile consisting of a two-layer soil medium above thick elastic bedrock as shown in Figure 1 is considered. The properties of each soil layer also vary horizontally and are modelled as three soil columns. The properties of soil layers, bed rock and source rock are presented in Table 1. There is an active fault of 20 km depth and 100 km away from the sites that may cause an earthquake with moment magnitude of 5.5.

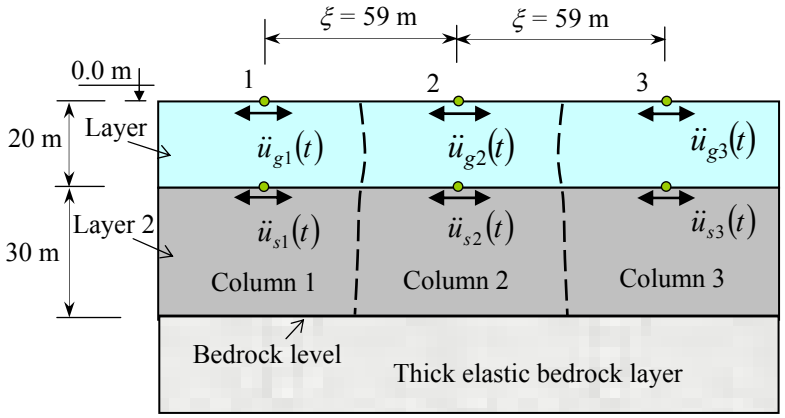

Figure 1. Geological profile of two-layer soil above thick elastic bedrock

The earthquake-induced horizontal motions of three surface sites (0, 0), (59, 0) and (118, 0), and three subsurface sites (0, -50), (59, -50) and (118, -50) on the interface of the two soil layers are simulated in this case study. The H-V 1986 coherency model parameters estimated at a separation distance of 59 m are $A = 0.0957$, $\alpha = 0.03727$, $\beta = 6.623$, $f_0 = 2.02$ Hz, and $k = 5.116\times10^4$ m (Dinh et al. 2012). The parameters of the amplitude- and frequency-modulation function (Chakraborty and Basu, 2008) presented in Table 2 are used for all sites ($j = 1, 2, 3$).

Table 1. Properties of soil layers, bed rock and source rock

Layer, depth	Soil Column	E [MN/m^2]	Poisson ratio ν	ρ [kN/m^3]	Damping ratio ξ [%]	V_s [m/s]
1, 20 m	1	24.6	0.23	17.9	0.45	74.0
	2	30.6	0.25	19.2	0.50	79.6
	3	21.6	0.22	18.3	0.35	68.9
2, 30 m	1	74.6	0.28	23.0	0.42	111.5
	2	70.6	0.27	22.5	0.40	110.1
	3	80.6	0.29	25.0	0.50	110.1
Bedrock		3000.0	0.25	2500	0.05	565.7
Source rock		70533.0	0.23	2800	0.02	3200

Table 2. Modulation parameters in different frequency bands (Chakraborty and Basu, 2008).

Band	Frequency limits (rad/s)		λ_j	β_j	γ_j
1	0.4953	0.5890	30.00164	0.0449	0.049121
2	0.5890	0.7005	29.84299	0.0824	0.090256
3	0.7005	0.8330	330.2238	0.1042	0.105069
4	0.8330	0.9907	16.9489	0.0916	0.107558
5	0.9907	1.1781	19.91785	0.0908	0.104127
6	1.1781	1.4010	35.31626	0.0746	0.080555
7	1.4010	1.6661	44.75151	0.0663	0.07044
8	1.6661	1.9813	39.51282	0.1001	0.107269
9	1.9813	2.3562	27.63662	0.2103	0.231993
10	2.3562	2.8020	67.13471	0.0843	0.087818
11	2.8020	3.3322	24.77418	0.1859	0.207441
12	3.3322	3.9626	122.3684	0.0598	0.06113
13	3.9626	4.7124	64.63215	0.1085	0.113203
14	4.7124	5.6040	53.86207	0.1517	0.159536
15	5.6040	6.6643	130.6111	0.1146	0.116974
16	6.6643	7.9253	80.4373	0.1882	0.194651
17	7.9253	9.4248	156.5035	0.0978	0.099483
18	9.4248	11.2080	92.96335	0.1346	0.138561
19	11.2080	13.3286	71.48464	0.2797	0.29051
20	13.3286	15.8505	72.47266	0.1316	0.136592
21	15.8505	18.8496	130.0072	0.0797	0.081399
22	18.8496	22.4160	101.9085	0.1170	0.120184
23	22.4160	26.6573	90.42829	0.0777	0.080038
24	26.6573	31.7010	75.27222	0.1819	0.188585
25	31.7010	37.6991	89.29339	0.1022	0.105359
26	37.6991	44.8321	81.59732	0.1761	0.182101
27	44.8321	53.3146	106.5307	0.1390	0.142596
28	53.3146	63.4021	163.8518	0.1659	0.168679

The time histories of simulated ground accelerations at site 1, site 2 and site 3 are shown in Figures 2a, 2c, and 2e, respectively. The time histories of simulated accelerations at the corresponding subsurface sites are shown in Figures 2b, 2d, and 2ef respectively. The spatial-variability and non-stationarities in both amplitude and frequency can be observed in those time histories. It is also seen that the periods of ground accelerations are longer than those of the subsurface motions whereas the acceleration amplitudes are almost equal.

The spatial-variability and temporal and spectral non-stationarities of the simulated accelerations are clearly observed in their squared wavelet coefficients shown in Figures 3. Both ground and subsurface accelerations are mainly contributed by the low-frequency components. The dominant frequency range for ground accelerations is 0-10 rad/s whereas that for subsurface accelerations is wider, 0-20 rad/s.

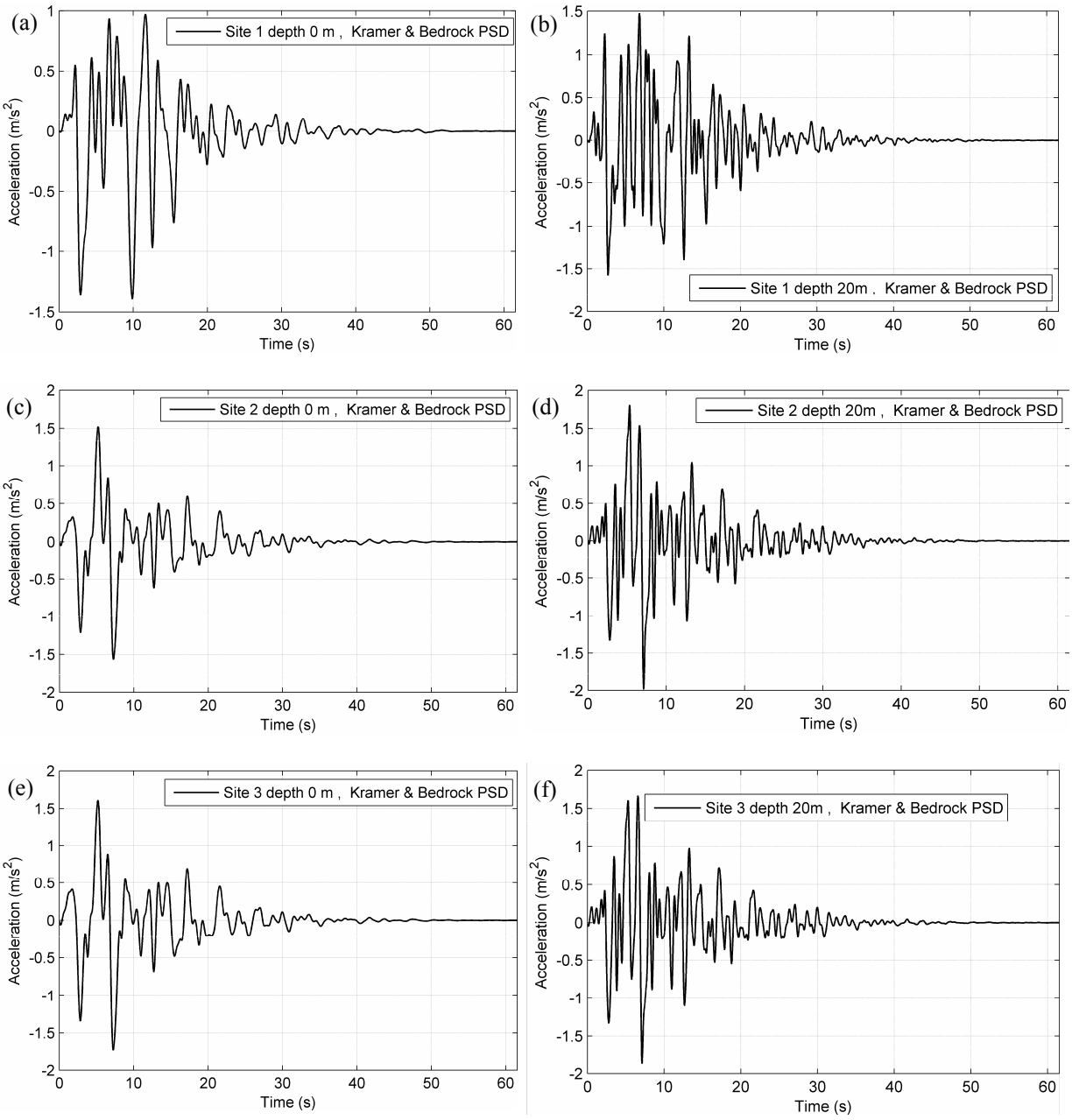

Figure 2. Time histories of simulated ground accelerations: (a) site 1, (c) site 2, (e) site 3; and subsurface accelerations (depth -20 m): (b) site 1, (d) site 2, (f) site 3.

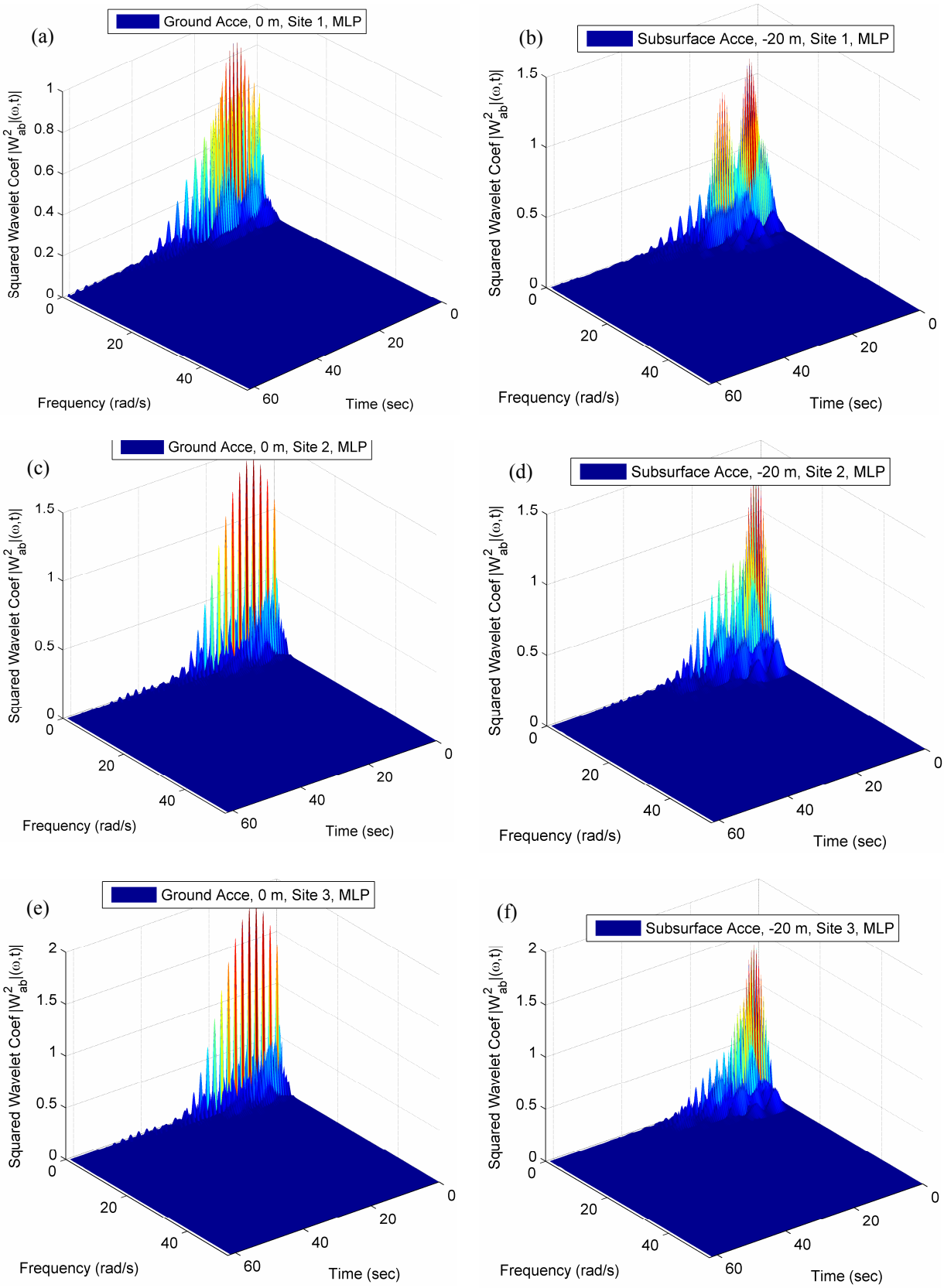

Figure 3. Squared wavelet coefficients of simulated ground accelerations: (a) site 1, (c) site 2, (e) site 3; and subsurface accelerations (depth -20 m): (b) site 1, (d) site 2, (f) site 3.

CONCLUSIONS

Simulations of spatially-varying non-stationary earthquake motions at subsurface sites in the multi-layered soil medium has been presented. The motions are compatible to the sites in both spatial-variation and earthquake energy content. The stochastic Fourier spectrum characterizing the energy accounts for source spectrum, attenuation, geometrical spreading and source-to-bedrock amplification. The bedrock and subsurface motions are related by a transfer function. The spatial-variation is represented by existing lagged coherency functional forms and their site-compatible parameters and uniform and random phases. Wavelet transform is introduced to investigate simultaneously the temporal and spectral variation of the simulated motions. In the case study, horizontal motions at three sites at ground surface and at a depth of 20 m in a two layered soil medium above the bedrock depth of 50 m and corresponding to an earthquake moment magnitude of 5.5 are simulated. The spatial-variability and temporal and spectral non-stationarities of the simulated accelerations are clearly observed in the squared wavelet coefficients where the low-frequency components are dominant.

ACKNOWLEDGEMENTS

This research is carried out under the EU FP7 funding for the Marie Curie IAPP project NOTES (Grant No. PIAP-GA-2008-230663). The authors are grateful for the support.

REFERENCES

Basu B. and Gupta V.K. (1998). Seismic response of SDOF system by wavelet modeling of non-stationary processes. *Journal of Engineering Mechanics*, ASCE, **124:10**, 1142-1150.

Boissières, H.P. and Vanmarcke, E.H. (1995). Estimation of lags for a seismograph array: wave propagation and composite correlation. *Soil Dynamics and Earthquake Engineering.* **14:1**, 5–22.

Boore, D. M. (2003). Simulation of Ground Motion Using the Stochastic Method. *Pure and Applied Geophysics.* **160**, 635–676.

Chakraborty, A and Basu B. (2008). Nonstationary response analysis of long span bridges under spatially varying differential support motions using continuous wavelet transform. *Journal of Engineering Mechanics*, ASCE. **134:2**, 155-162.

Deodatis, G. (1996). Non-stationary Stochastic Vector Processes: Seismic Ground Motion Applications, *Probabilistic Engineering Mechanics.* **11**, 149-168.

Dinh, V.N., Basu, B., and Brinkgreve, R.B.J. (2012). Non-stationary Response of Spatially-Extended Structures, Project Report, Plaxis BV, Delft and Trinity College Dublin.

Harichandran, R.S. and Vanmarcke, E.H. (1986). Stochastic Variation of Earthquake Ground Motion in Space and Time, *ASCE J. Eng. Mech. Div*. **112:2**, 154–174.

Konakli, K. and Der Kiureghian A. (2011). Simulation of spatially varying ground motions including incoherence, wave-passage and site-response effects. *Earthquake Engineering and Structural Dynamics*. **41:3**, 495-513.

Kramer, S.L. (1996), Geotechnical Earthquake Engineering, Prentice Hall, New Jersey, USA.

Zerva, A. (2009). Spatial Variation of Seismic Ground Motions: Modelling and Engineering Applications, Taylor & Francis Group LLC: Boca Raton.